Deterministic Retrieval of Complex Green's Functions Using Hard X Rays

D. J. Vine,[1,*] D. M. Paganin,[1] K. M. Pavlov,[1,2,3] K. Uesugi,[4] A. Takeuchi,[4] Y. Suzuki,[4] N. Yagi,[4] T. Kämpfe,[5] E.-B. Kley,[5] and E. Förster[6]

[1]*School of Physics, Monash University, VIC 3800, Australia*
[2]*Monash Centre for Synchrotron Science, Monash University, VIC 3800, Australia*
[3]*School of Science and Technology, University of New England, NSW 2351, Australia*
[4]*Japan Synchrotron Radiation Research Institute (JASRI), SPring-8, Hyogo 679-5198, Japan*
[5]*Institute of Applied Physics, Friedrich-Schiller University, Jena 07743, Germany*
[6]*Institute of Optics and Quantum Electronics, Friedrich-Schiller University, Jena 07743, Germany*

(Received 3 March 2008; revised manuscript received 21 December 2008; published 26 January 2009)

A massively parallel deterministic method is described for reconstructing shift-invariant complex Green's functions. As a first experimental implementation, we use a single phase contrast x-ray image to reconstruct the complex Green's function associated with Bragg reflection from a thick perfect crystal. The reconstruction is in excellent agreement with a classic prediction of dynamical diffraction theory.

DOI: 10.1103/PhysRevLett.102.043901 PACS numbers: 42.30.Lr, 42.25.Fx, 42.40.−i

The Green's function in coherent optics is used to describe the effect of an optical system (e.g., propagation through free space) on the phase and amplitude of a complex exit surface wave (ESW). The Green's function, however, being a complex quantity, cannot be measured directly despite the practical importance of such a measurement.

In this Letter, we will present a general approach which allows us to reconstruct complex, shift-invariant Green's functions using a method inspired by holography. In our approach, the holographic interference between reference and scattered beams is replaced with a general optical system which causes phase and amplitude contrast in the associated output field. By recording a hologram of a known object, we reconstruct the complex Green's function of an unknown optical system.

The ability to reconstruct Green's functions from experimental data has applications in a broad range of physics disciplines. For example, reconstructing the Green's function in a holography experiment using electromagnetic or matter wave fields would allow the Helmholtz or Schrödinger propagators, respectively, to be reconstructed [1]. Furthermore, one can imagine the importance of directly reconstructing the complex Green's function associated with isoplanatic regions [2] of lenses in light or electron microscopy to diagnose aberrations [3] or the Green's function associated with linear Fresnel zone plates used in nanoprobe focusing of x rays [4].

To demonstrate our Green's-function reconstruction approach, we will present the experimental reconstruction of the x-ray Green's function associated with Bragg reflection from a thick perfect crystal. While we have chosen to exemplify this method on a specific coherent x-ray application, we stress that it can be used for coherent electromagnetic or matter wave fields and a wide class of shift-invariant Green's functions.

Further to our previous comments on the applications of Green's-function reconstruction, as we shall show in this Letter, by experimentally reconstructing the Green's function associated with diffraction from a perfect crystal, we can verify the classic predictions of the dynamical diffraction theory of Darwin, Ewald, and von Laue [5]. At the same time, our approach can be used to give an analytic solution to the famous one-dimensional phase problem first formulated by Pauli in the context of quantum mechanics [6].

The essence of our approach to reconstruct Green's functions is illustrated in the following example. Consider the classic description of wave-field evolution in terms of a shift-invariant Green's function G [7]:

$$\Psi(\mathbf{r}) = \int G(\mathbf{r} - \mathbf{r}')\psi(\mathbf{r}')d\mathbf{r}', \tag{1}$$

where Ψ and ψ describe coherent complex scalar wave fields and $\mathbf{r}$ is a position vector. The problem is to solve Eq. (1) for G given knowledge of $|\Psi|$ and ψ; in general, this is a highly nonlinear inverse problem. The problem can be linearized without compromising the generality of G by choosing ψ to have the property that $\psi(\mathbf{r}) = 1 + \eta(\mathbf{r})$, where $|\eta(\mathbf{r})| \ll 1$—the so-called "weak object" property [3]. Under these conditions, it is possible, as we shall show, to solve Eq. (1) for G analytically.

We now turn to the specific problem of reconstructing the Green's function associated with hard-x-ray Bragg reflection from a perfect crystal. The analysis that follows is easily generalizable to the other optical systems mentioned previously. The Green's function of perfect crystal Bragg reflection [5] is one-dimensional, which means it can be recovered from a single two-dimensional intensity measurement (reconstruction of two-dimensional complex Green's functions require two measurements, in general).

Before we turn to the analysis, a brief comment that speaks to the utility of Green's-function retrieval: While

we have chosen this system as a means for demonstrating our Green's-function retrieval technique, we note that in the regime of kinematic diffraction from the crystal our approach unambiguously solves the famous one-dimensional phase problem hitherto partially addressed by the following techniques: Hilbert transform [8], methods based on photoelectron emission due to x-ray standing waves [9] and Fourier analysis techniques [10].

With reference to Fig. 1, we now explain the reconstruction algorithm in more detail [11]. Depicted is a planar monochromatic scalar hard-x-ray wave field propagating through the weak object and imaging system to the two-dimensional detector. The inset gives the specific case for symmetric Bragg reflection from a perfect crystal. A simple coordinate transform, the details of which are omitted for clarity, renders the diffracted beam collinear with the incident beam.

The weak object ESW $\psi(\mathbf{r}_\perp, z = 0)$ is the product of the incident plane wave and its complex transmission function. The weak object is composed of a single material with refractive index decrement δ, attenuation coefficient β, and projected thickness $T(\mathbf{r}_\perp)$ [12]. We require

$$\psi(\mathbf{r}_\perp, 0) = \exp[-kn_T T(\mathbf{r}_\perp)] \approx \exp[-kn_T \bar{T}][1 - kn_T \Delta T(\mathbf{r}_\perp)], \quad (2)$$

where $n_T = i\delta + \beta$, $\mathbf{r}_\perp = (x, y)$, $\mathbf{k}_\perp = (k_x, k_y)$ is the dual to $\mathbf{r}_\perp$, $k = 2\pi/\lambda = |(\mathbf{k}_\perp, k_z)|$, λ is the radiation wavelength, and $T(\mathbf{r}_\perp) = \bar{T} + \Delta T(\mathbf{r}_\perp)$, where $\bar{T}$ and ΔT denote average thickness and deviation from the average thickness, respectively. The approximation in Eq. (2) is valid when $|\delta k \Delta T(\mathbf{r}_\perp)| \ll 1$, $|\beta k \Delta T(\mathbf{r}_\perp)| \ll 1$, and we now briefly digress from the analysis to show how this may be achieved in practice.

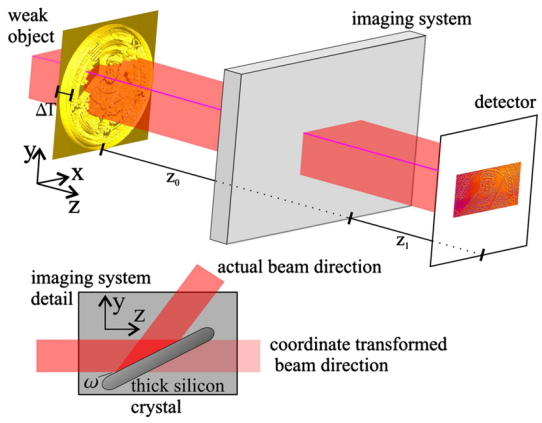

FIG. 1 (color online). Experimental reconstruction of a generic complex Green's function. Coherent plane waves illuminate a weak object before propagating a distance z_0 to the imaging system. The inset shows the imaging system for the case of x-ray Bragg reflection from a thick perfect silicon crystal. The field exiting the imaging system propagates a further distance z_1 to the detector. This single intensity image may be deterministically inverted to recover the complex Green's function associated with the shift-invariant imaging system.

Splitting the arguments of Eq. (2) into a real part $\mu = k\beta\Delta T$ and an imaginary part $\varphi = -k\delta\Delta T$, it may be written [13]

$$\psi(\mathbf{r}_\perp, 0) = \exp(i\bar{\varphi} - \bar{\mu})[1 + i\Delta\varphi(\mathbf{r}_\perp) - \Delta\mu(\mathbf{r}_\perp)]. \quad (3)$$

It is necessary that $|\Delta\mu|$ and $|\Delta\varphi|$ be of the same order of magnitude; however, for most materials, the x-ray refractive index decrement δ is 3 orders of magnitude greater than the attenuation coefficient β. We overcome the problem by allowing the wave field to propagate before it is incident on the crystal [12,14–18]. The distance z_0 (see Fig. 1) is increased so that the curvature in the wave front, due to the weak object, causes neighboring rays to interfere, producing intensity variations that are tantamount to increasing β. For small z, the propagation-induced contrast is proportional to the transverse Laplacian $\nabla_\perp^2 = \frac{\partial^2}{\partial x^2} + \frac{\partial}{\partial y^2}$ of $\Delta\varphi(\mathbf{r}_\perp, 0)$ [12] and can be considered an effective attenuation over the plane $z = z_0$.

Returning to the main thread of the analysis, Eq. (3) makes clear the connection of this approach to holography: The weak object ESW $\psi(\mathbf{r}_\perp, z = 0)$ is the sum of the direct beam and a known weak perturbation. Reflection from the crystal will modulate the amplitude and phase of the field, and the detector records the hologram. The hologram evidently contains the response of the imaging system to all spatial frequencies present in ψ, which allows a massively parallel interrogation of a wide range of reciprocal space simultaneously. We will now show how to invert the hologram to recover the Green's function.

The intensity recorded on the detector is [13]

$$I(\mathbf{r}_\perp, z_0 + z_1; \omega) = \bar{I}(|\tilde{G}(0, \omega)|^2 + 2\mathrm{Re}\{\tilde{G}^*(0; \omega) \times \int G(\mathbf{r}_\perp - \mathbf{r}'_\perp; \omega)[i\Delta\varphi(\mathbf{r}'_\perp) - \Delta\mu(\mathbf{r}'_\perp)]d\mathbf{r}'_\perp\}). \quad (4)$$

Here $I(\mathbf{r}_\perp, z) = |\Psi(\mathbf{r}_\perp, z)|^2$, ω is the angle between the direct x-ray beam and crystal surface (a constant), μ and φ now refer to attenuation and phase of the propagated wave field, respectively, $*$ denotes complex conjugation, and $\bar{I} = \exp(-2\bar{\mu})$. Terms quadratic in the small quantities $\Delta\mu$ and $\Delta\varphi$ are discarded as negligible, together with the effects of short propagation distance z_1—valid for large Fresnel numbers [12]. $\tilde{G}(0, \omega)$ is a single complex number (given that ω was held constant during the measurement) which represents the ratio of dc values of Ψ to ψ, a known quantity.

With a view to deriving an expression for $G(\mathbf{r}_\perp; \omega)$, we introduce the known contrast function $C(\mathbf{r}_\perp, z; \omega) = I(\mathbf{r}_\perp, z; \omega)/\bar{I} - |\tilde{G}(0, \omega)|^2$ and scale the Green's function $\Gamma(\mathbf{r}_\perp; \omega) = G(\mathbf{r}_\perp; \omega)\tilde{G}^*(0, \omega)$. We will now use a one-dimensional Fourier transform, and so to clarify the analysis we write the vectors $\mathbf{r}_\perp$ and $\mathbf{k}_\perp$ explicitly in terms of their Cartesian components. Equation (4) becomes, after a one-dimensional Fourier transform,

$$-\tilde{C}(x, z_0 + z_1; k_y, \omega) = [\Delta\tilde{\mu}(x; k_y) - i\Delta\tilde{\varphi}(x; k_y)]\tilde{\Gamma}(k_y, \omega) + [\Delta\tilde{\mu}(x; k_y) + i\Delta\tilde{\varphi}(x; k_y)] \times \tilde{\Gamma}^*(-k_y, \omega), \quad (5)$$

where the Fourier transform is defined by $\tilde{G}(x; k_y) = \int G(x, y)\exp(-ik_y y)dy$.

Equation (5) is linear in the unknown complex function $\tilde{\Gamma}(k_y, \omega)$, which can be solved for using any two discrete lines (i, j) of the image:

$$\begin{pmatrix} \tilde{\Gamma}_R^e \\ \tilde{\Gamma}_R^o \\ \tilde{\Gamma}_I^e \\ \tilde{\Gamma}_I^o \end{pmatrix} = -\frac{1}{2}\begin{pmatrix} \Delta\tilde{\mu}_R^i & \Delta\tilde{\varphi}_I^i & \Delta\tilde{\varphi}_R^i & -\Delta\tilde{\mu}_I^i \\ \Delta\tilde{\mu}_I^i & -\Delta\tilde{\varphi}_R^i & \Delta\tilde{\varphi}_I^i & \Delta\tilde{\mu}_R^i \\ \Delta\tilde{\mu}_R^j & \Delta\tilde{\varphi}_I^j & \Delta\tilde{\varphi}_R^j & -\Delta\tilde{\mu}_I^j \\ \Delta\tilde{\mu}_I^j & -\Delta\tilde{\varphi}_R^j & \Delta\tilde{\varphi}_I^j & \Delta\tilde{\mu}_R^j \end{pmatrix}^{-1}\begin{pmatrix} \tilde{C}_R^i \\ \tilde{C}_I^i \\ \tilde{C}_R^j \\ \tilde{C}_I^j \end{pmatrix}, \quad (6)$$

where R, I, e, and o refer to the real, imaginary, even, and odd parts of the relevant function, respectively. The solution makes use of an *a priori* known symmetry that in the case of a laterally homogeneous crystal the Green's function is one-dimensional. In this case, a pair of discrete lines of the image contains all of the information we seek to retrieve; since there are many such lines in the output of a conventional two-dimensional detector, we may perform a suitable average to greatly reduce noise artifacts. Equation (6) is the unambiguous deterministic solution for the complex Green's function we were seeking, and we now present the experimental reconstruction applied to a thick perfect silicon crystal.

The problem, as stated previously and solved by Eq. (6), is to reconstruct G given $\psi(\mathbf{r}_\perp, z = z_0)$ and $|\Psi(\mathbf{r}_\perp, z = z_0 + z_1)|$, and so we must now account for how the two latter *known* quantities are measured. Clearly, $|\Psi(\mathbf{r}_\perp, z_0 + z_1)|$ can be measured by recording the intensity in the manner specified by Fig. 1, but $\psi(\mathbf{r}_\perp, z = z_0)$ is a complex quantity, the phase of which cannot be measured directly. The magnitude $|\psi(\mathbf{r}_\perp, z_0)|$ is easily measured by placing the detector at the plane z_0—this was done, and Fig. 2(a) is the result. The phase of $\psi(\mathbf{r}_\perp, z_0)$ was calculated from Fig. 2(a) using the single-image transport-of-intensity phase-retrieval algorithm [19], and the result is shown in Fig. 2(b). The remaining input $|\Psi(\mathbf{r}_\perp, z_0 + z_1)|$ discussed previously is shown in Fig. 2(c).

The weak object was fabricated by etching a binary pattern [20] of 0.8 μm depth (400 nm lateral resolution) into a 0.8 mm thick SiO_2 substrate using electron beam lithography. The aperiodic pattern ensures that the weak object ESW will have a continuous spatial Fourier spectrum. The experiments were conducted at the BL20XU undulator beam line at SPring-8 (Japan) using 20 keV x rays from a double Si (111) monochromator. The beam size was approximately 4(hor) $\times$ 2(ver) mm at 245 m from the source; $z_0 = 1.2$ m and $z_1 = 0.06$ m. Images were recorded using a Hamamatsu CCD detector coupled to an optical lens and phosphor screen with a 0.9 μm effective pixel size and 2(hor) $\times$ 1.3(ver) mm field of view. The x-ray beam from the undulator source is partially coherent, and this has been shown to deleteriously affect reconstruction algorithms that assume fully coherent incident radiation [21].

Figure 2(c) was measured with the crystal slightly detuned from the (111) Bragg reflection so that 70% of the direct beam was reflected. The vertical elongation of Fig. 2(c) indicates the crystal was cut asymmetrically by 0.8° to the (111) plane—the correction of which was accounted for in the reconstruction algorithm. Figure 2 represents all of the inputs to the algorithm of Eq. (6) that allow reconstruction of G.

The results of the reconstruction are presented in Figs. 3(a) and 3(b), which show the reconstructed squared modulus and phase of the thick perfect silicon analyzer crystal Green's function using Eq. (6) compared to the classic prediction of dynamical diffraction [5]. The two are in excellent agreement. The discrepancy between the predicted Green's function and the reconstruction merits further discussion, which we turn to now.

The gray shaded regions in Fig. 3 show the condition number of the inverse matrix in Eq. (6) and represent the region of validity of the reconstruction. A large condition number indicates that the output of Eq. (6) varies significantly upon a small change in the input, and so at this point the solution is numerically unstable. At high spatial frequencies, the large condition number is due to the low power scattered into these frequencies. The large condition

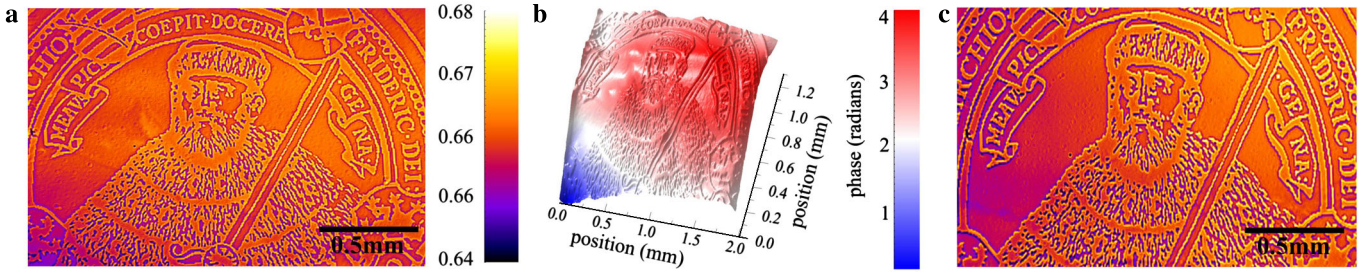

FIG. 2 (color online). (a) Intensity measurement prior to reflection from the crystal showing only propagation phase contrast; (b) calculated phase corresponding to (a); (c) measured intensity image showing the image of the weak object after reflection from a thick perfect silicon crystal (111) reflection. The crystal was slightly detuned from the Bragg condition so that it reflects 70% of the direct beam.

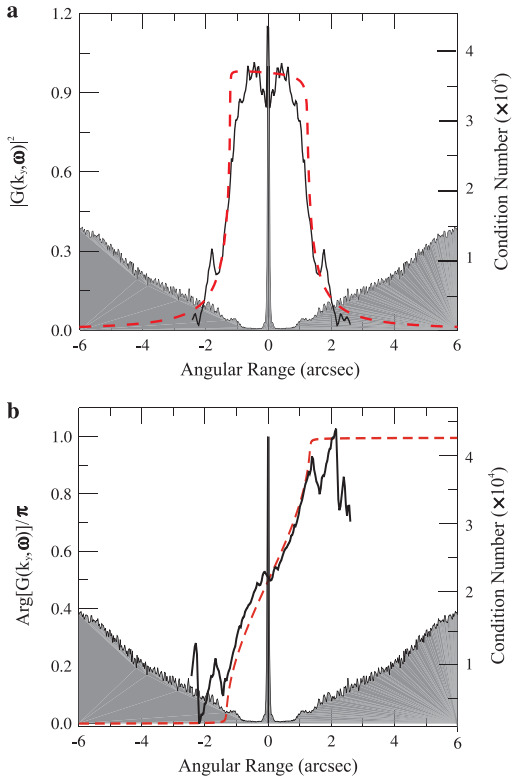

FIG. 3 (color online). (a) $|G(k_y, \omega)|^2$—squared magnitude of the reconstructed Green's function for the silicon analyzer crystal (solid black line) and theoretical prediction (broken red line), (b) Arg$[G(k_y, \omega)]$—phase corresponding to (a). The condition number of the solution is shown for each angular space point.

number around the $0''$ point in Figs. 3(a) and 3(b) is due to the manner in which the algorithm reconstructs the Green's function by separating it into even and odd functions. The odd functions in Eq. (6) ($\tilde{\Gamma}_R^o$, $\tilde{\Gamma}_I^o$) must approach zero in the vicinity of $0''$, and the resulting matrix inversion at these angular space points renders the solution more susceptible to noise in the experimental data.

The angular range of the single image reconstruction is Nyquist limited by the detector pixel size. The angular resolution of the reconstruction is inversely proportional to the number of pixels used in the image. The reconstructions in Fig. 3 were calculated using a 512 square pixel subimage of Fig. 2 yielding an angular resolution at least equal to high resolution x-ray diffraction. This approach is sensitive to misalignment of the images which must be achieved to single pixel accuracy.

In conclusion, we have demonstrated the validity of our new technique for reconstructing shift-invariant complex Green's functions. The reconstructed Green's function associated with reflection from a perfect single crystal of silicon quantitatively agrees with the classic prediction of the dynamical theory of x-ray diffraction for perfect crystals [5]. While the experiment we have presented is specifically related to crystallography, we note that the technique is applicable to a very wide class of complex Green's functions. The technique as demonstrated here uses only a single intensity image or probability density, after the weak object has been characterized, and as such is suitable to tomographic and real-time applications.

D. J. V. acknowledges the German Academic Exchange Service (DAAD) and support from the Australian government. K. M. P. acknowledges support from the Monash Centre for Synchrotron Science Fellowships program. D. J. V., D. M. P., and K. M. P. acknowledge funding from the Australian Research Council (ARC) and Access to Major Research Facilities (AMRF). The synchrotron radiation experiments were performed with the approval of the Japan Synchrotron Radiation Research Institute (JASRI) (Proposal No. 2007A1173-NL-np).

*dvine@unimelb.edu.au

[1] R. P. Yu, D. M. Paganin, and M. J. Morgan, Phys. Lett. A **341**, 156 (2005).
[2] M. Born and E. Wolf, *Principles of Optics* (Cambridge University Press, Cambridge, England, 1999), 7th ed.
[3] J. M. Cowley, *Diffraction Physics* (North-Holland, Amsterdam, 1995), 3rd ed.
[4] H. C. Kang, J. Maser, G. B. Stephenson, C. Liu, R. Conley, A. T. Macrander, and S. Vogt, Phys. Rev. Lett. **96**, 127401 (2006).
[5] A. Authier, *Dynamical Theory of X-Ray Diffraction* (Oxford University Press, Oxford, 2005), revised ed.
[6] W. Pauli, *Handbuch der Physik* (Springer, Berlin, 1933).
[7] J. D. Jackson, *Classical Electrodynamics* (Wiley, New York, 1998), 3rd ed.
[8] P. V. Petrashen' and F. N. Chukhovskii, Sov. Phys. Dokl. **34**, 957 (1989).
[9] A. M. Afanas'ev and V. G. Kon, Sov. Phys. JETP **47**, 154 (1978).
[10] S. G. Podorov, V. I. Punegov, and V. A. Kusikov, Phys. Solid State **36**, 454 (1994).
[11] D. J. Vine, D. M. Paganin, K. M. Pavlov, and S. G. Podorov, J. Appl. Crystallogr. **40**, 650 (2007).
[12] D. M. Paganin, *Coherent X-Ray Optics* (Oxford University Press, New York, 2006).
[13] Ya. I. Nesterets, T. E. Gureyev, D. Paganin, K. M. Pavlov, and S. W. Wilkins, J. Phys. D **37**, 1262 (2004).
[14] A. A. Snigirev, I. I. Snigireva, V. G. Kohn, S. Kuznetsov, and I. A. Schelokov, Rev. Sci. Instrum. **66**, 5486 (1995).
[15] S. W. Wilkins, T. E. Gureyev, D. Gao, A. Pogany, and A. W. Stevenson, Nature (London) **384**, 335 (1996).
[16] P. Cloetens, R. Barrett, J. Baruchel, J.-P. Guigay, and M. Schlenker, J. Phys. D **29**, 133 (1996).
[17] D. Paganin and K. A. Nugent, Phys. Rev. Lett. **80**, 2586 (1998).
[18] K. A. Nugent, T. E. Gureyev, D. F. Cookson, D. Paganin, and Z. Barnea, Phys. Rev. Lett. **77**, 2961 (1996).
[19] D. M. Paganin, S. C. Mayo, T. E. Gureyev, P. R. Miller, and S. W. Wilkins, J. Microsc. **206**, 33 (2002).
[20] Johann Frederick (der Grossmuetige), founder of Friedrich-Schiller University.
[21] Ya. I. Nesterets, T. E. Gureyev, and S. W. Wilkins, J. Phys. D **38**, 4259 (2005).